

Substituted Phenanthrolines

A Quantitative Description of the σ -Donor and π -Acceptor Properties of Substituted PhenanthrolinesG. Attilio Ardizzoia,^[a] Michela Bea,^[a] Stefano Brenna*^[a] and Bruno Therrien^[b]

Abstract: The bond between molybdenum and substituted 1,10-phenanthroline ligands in a series of $[\text{Mo}(\text{CO})_4(\text{phen}^*)]$ complexes has been studied by combining experimental data (ν_{CO}) with DFT calculations. First, natural orbitals for chemical valence (NOCV) were calculated: The resulting charge-transfer magnitudes (Δq_i) associated with the deformation density channels ($\Delta \rho_i$) were related to σ -donation and π -back-donation. Then, energy decomposition analysis was performed by applying the extended transition state (ETS) scheme. The outcomes of the ETS-NOCV approach has allowed us to quantify the ener-

getic contribution of both ligand-to-metal (E_σ) and metal-to-ligand (E_π) interactions. A new parameter (T^{phen}) has been introduced comprising both E_σ and E_π and thus providing a descriptor for the overall electronic contribution given by phenanthrolines to the metal–ligand bond. This was corroborated by the linear correlation found between T^{phen} and the ν_{CO} vibration modes of $[\text{Mo}(\text{CO})_4(\text{phen}^*)]$ complexes, at least for those containing a 2,9-unsubstituted phenanthroline. The case of $[\text{Mo}(\text{CO})_4(\text{phen}^*)]$ derivatives with a 2,9-substituted phen* is also discussed.

Introduction

Understanding the nature of metal–ligand bonds in transition-metal complexes is of crucial importance in organometallic chemistry^[1] and hence both experimental^[2] and theoretical^[3] studies have been performed in this area over the last decades. Different theoretical approaches have been applied to the description of the donor–acceptor properties of ligands in transition-metal complexes, for example, interaction-energy partitioning schemes,^[4] charge decomposition analysis (CDA),^[5] constrained space orbital variation (CSOV),^[6] natural bond orbital (NBO),^[7] molecular electrostatic potential (MEP),^[8] and quantitative analysis of ligand effect (QALE).^[9] More recently, Mitoraj and co-workers introduced natural orbitals for chemical valence (NOCV),^[10] a singular approach that gives an accurate description of bonding in terms of only a few orbitals localized in the bonding region. In addition, this method allows for the separation of the contributions to the deformation density ($\Delta \rho$) arising from the ligand-to-metal and metal-to-ligand electron-transfer processes, thus being closely related to the Dewar–Chatt–Duncanson model usually applied to organometallic compounds. Furthermore, when NOCV is associated with an energy decomposition analysis scheme [in particular with the extended transition state (ETS) method, initially developed by Ziegler and Rauk^[11]], it is possible to give a quantitative (i.e., energetic) description of the σ -donor (E_σ) and π -acceptor (E_π) contributions to the metal–ligand bond. Thus, in the last years,

the ETS-NOCV approach has emerged as a very precious tool for shedding light on the nature of metal-to-ligand interactions, as documented in the different cases studied.^[12–31] In the present study, we applied ETS-NOCV to a series of $[\text{Mo}(\text{CO})_4(\text{phen}^*)]$ complexes (phen* = substituted 1,10-phenanthroline) with the purpose of describing and quantifying the σ -donor and π -acceptor properties of phen* depending on their substitution. Among others, 1,10-phenanthrolines form a ubiquitous, significant class of ligands^[32] that find application as fluorescent receptors,^[33] antennae in luminescent metal complexes,^[34] and in the synthesis of highly emitting phosphorescent compounds,^[35] to name but a few. In particular, $[\text{M}(\text{CO})_4(\text{phen}^*)]$ compounds (M = Cr, Mo, W) have been the subject of extensive reports dealing with their electrochemical behavior,^[36] photo-physical properties,^[37] photochemical reactivity,^[38] and use as catalysts.^[39] As highlighted by Farrell et al.,^[37c] due to their structural simplicity and the presence of CO ligands, the IR bands of which are sensitive markers for electron-density distribution, Group 6 metal carbonyls are an excellent model for studying how ligand substituents affect the physicochemical properties of compounds. Indeed, in a detailed study on $[\text{M}(\text{CO})_4(\text{N},\text{N})]$ complexes (M = Cr, W; N,N = 1,10-phenanthroline, 3,4,7,8-tetramethyl-1,10-phenanthroline), they performed TD-DFT calculations to estimate the influence of the substitution of phenanthrolines on electronic spectra. Herein, we report the description of the bond between molybdenum and 1,10-phenanthrolines in terms of the σ -donor (E_σ) and π -acceptor (E_π) contributions of the nitrogen heterocycle. Applying the ETS-NOCV model to several $[\text{Mo}(\text{CO})_4(\text{phen}^*)]$ systems, it has been possible to quantify these contributions and to correlate E_σ and E_π of the different phenanthrolines with experimental values of carbonyl stretching vibrations (ν_{CO}) obtained for the corresponding complexes in solution. A new parameter, T^{phen} , which simultaneously takes into account both σ -donation (E_σ) and π -

[a] Department of Science and High Technology, University of Insubria, Via Valleggio, 9 22100 Como, Italy
E-mail: stefano.brenna@uninsubria.it
<http://www.uninsubria.it/docenti/stefano.brenna>

[b] Institute of Chemistry, University of Neuchâtel, Avenue de Bellevaux 51, 2000 Neuchâtel, Switzerland

Supporting information and ORCID(s) from the author(s) for this article are available on the WWW under <http://dx.doi.org/10.1002/ejic.201600647>.

back-bonding (E_{π}) along the metal–phen* bond, has been defined, and a linear correlation between T^{phen} and the experimental ν_{CO} frequencies has been demonstrated.

Results and Discussion

Syntheses

The 1,10-phenanthrolines used in this study (Figure 1) differ in the nature of the substituents (H, CH₃, Ph, NO₂, NH₂, Cl, Br, CN) or in their position on the phenanthroline backbone. Most of phen* derivatives were purchased, but 5-NO₂-phen^[40] and 5-NH₂-phen^[33] were prepared according to procedures reported in the literature. The complexes [Mo(CO)₄(phen*)] (**1–16**) were synthesized^[41] by heating in toluene molybdenum hexacarbonyl with 1 equivalent of ligand (Scheme 1). The reactions were easily monitored by IR spectroscopy, in which the characteristic band of [Mo(CO)₆] at 1980 cm⁻¹ was replaced by four CO stretching vibrations (ν_{CO}), characteristic of a *cis*-[Mo(CO)₄(L)₂] system^[37c] (Figure 2). The values of the $A_{1\text{ax}}$, B_1 , $A_{1\text{eq}}$ and B_2 modes of compounds **1–16**, recorded in dichloromethane solution, are collected in Table 1.

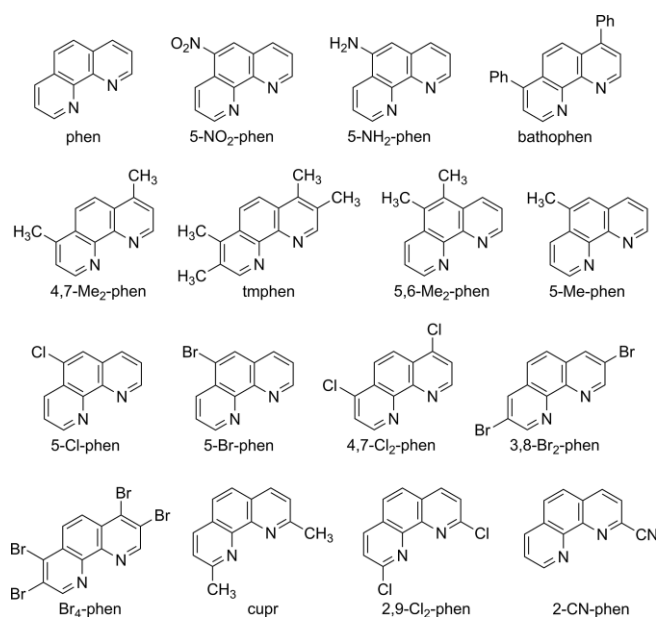
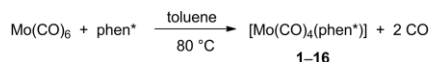


Figure 1. Substituted 1,10-phenanthrolines studied in this work, with the corresponding abbreviations used throughout the paper.



phen*:	1 phen	5 4,7-Me ₂ -phen	9 5-Cl-phen	13 Br ₄ -phen
	2 5-NO ₂ -phen	6 tmphen	10 5-Br-phen	14 cupr
	3 5-NH ₂ -phen	7 5,6-Me ₂ -phen	11 4,7-Cl ₂ -phen	15 2,9-Cl ₂ -phen
	4 bathophen	8 5-Me-phen	12 3,8-Br ₂ -phen	16 2-CN-phen

Scheme 1. Syntheses of [Mo(CO)₄(phen*)] complexes **1–16**.

As can be seen from the data in Table 1, the electronic effect imposed by ligand phen* is reflected in all the ν_{CO} vibrational modes. This is best explained in Figures S1–S3 in the Supporting Information: A good linear relationship among the different

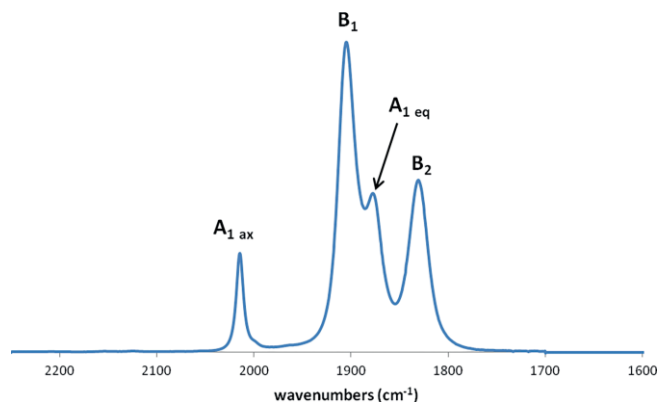


Figure 2. IR spectrum of [Mo(CO)₄(phen)] (**1**) in dichloromethane, with assignment of vibrational bands.

Table 1. IR frequencies recorded for compounds **1–16** in dichloromethane.

	phen*	ν_{CO} [cm ⁻¹]			
		$A_{1\text{ax}}$	B_1	$A_{1\text{eq}}$	B_2
1	phen	2015.1	1905.3	1878.0	1831.3
2	5-NO ₂ -phen	2017.4	1910.6	1884.4	1837.3
3	5-NH ₂ -phen	2014.1	1904.0	1877.2	1830.1
4	bathophen	2013.9	1904.7	1877.2	1830.2
5	4,7-Me ₂ -phen	2013.7	1902.2	1874.2	1827.8
6	tmphen	2013.1	1900.5	1872.4	1825.3
7	5,6-Me ₂ -phen	2014.2	1904.1	1876.4	1830.0
8	5-Me-phen	2014.7	1904.9	1877.3	1830.4
9	5-Cl-phen	2016.3	1907.8	1881.0	1834.2
10	5-Br-phen	2016.2	1907.8	1880.9	1834.1
11	4,7-Cl ₂ -phen	2017.0	1909.7	1883.1	1836.0
12	3,8-Br ₂ -phen	2018.0	1912.2	1886.6	1839.5
13	Br ₄ -phen	2019.3	1915.8	1891.3	1844.4
14	cupr	2016.9	1904.9	1875.3	1825.3
15	2,9-Cl ₂ -phen	2019.0	1909.6	1887.6	1839.1
16	2-CN-phen	2018.8	1913.8	1894.8	1846.8

sets of values (i.e., $A_{1\text{ax}}$ vs. B_1 etc.) is observed, with the exception of species containing 2,(9)-substituted phen* ligands **14–16**, which repeatedly deviate from the lines in Figures S1–S3. The odd behavior of compounds **14–16** can be reasonably ascribed to the steric hindrance induced by 2,9-substitution, which is reflected by the greater deviation in those graphs in which a vibration mainly associated with equatorial carbonyls ($A_{1\text{eq}}$, B_2) is involved. In view of this discrepancy, compounds **14–16** were first excluded from our study (and will be considered at the end of the discussion), applying the ETS-NOCV method only on complexes **1–13**.

Geometry Optimization

As stated in the Introduction, the ETS-NOCV approach gives a quantitative description of the bonding in terms of only a few orbitals localized in the metal–ligand bonding region, allowing quantification of the σ -donor and π -acceptor properties of a ligand. The first step in this method is the optimization of the geometries of the complexes under investigation. In the present study we employed the hybrid functional PBE0,^[42] which previously proved to give computational results consistent with the experimental data.^[43] Taking into consideration

the complex $[\text{Mo}(\text{CO})_4(\text{phen})]$ (**1**) as a paradigmatic example of the series **1–13**, its molecular structure was optimized starting from the X-ray data taken from the literature.^[44] The computed results showed good agreement with the experimental data (Figure 3, left and Table S1 in the Supporting Information). Thus, the same procedure was extended to the remaining complexes by using the X-ray crystal structure of **1** as the starting point to optimize the geometries of **2–13**. The results of the geometry optimizations of all the complexes are reported in the Supporting Information.

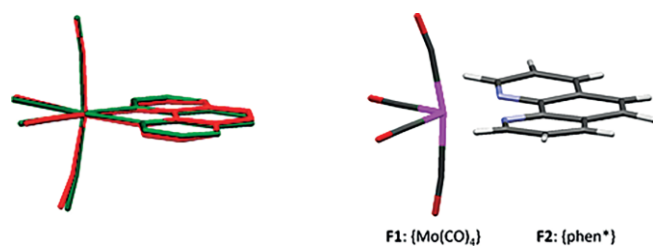


Figure 3. Left: Comparison between the molecular structure of $[\text{Mo}(\text{CO})_4(\text{phen})]$ (**1**) obtained by X-ray diffraction analysis (red) and after geometry optimization (green; RMSD = 0.1166). Right: Definition of the fragments used to calculate the NOCV for complexes **1–13**.

NOCV Calculations

The optimized structures were used to calculate the corresponding NOCV, fragmenting the whole molecule into two subsystems, **F1** (the $\{\text{Mo}(\text{CO})_4\}$ fragment) and **F2** (the phen* ligand), as illustrated in Figure 3 (right). All species showed similar features as regards the description of the bond interaction between **F1** and **F2**, and they will be discussed in relation to $[\text{Mo}(\text{CO})_4(\text{phen})]$ (**1**). The results of these calculations are NOCVs that are defined as the eigenvectors that diagonalize the deformation density matrix and are obtained as a pair of eigenfunctions $\varphi_{\pm k}$ corresponding to eigenvalues ν_k and ν_{-k} with the same absolute value but of opposite sign. As it is usually the case, it is more convenient to visualize the deformation density ΔQ_k [Equation (1)] associated with each pair of eigenvalues $\nu_{\pm k}$.

$$\Delta Q_k = -k\varphi_{-k}^2 + k\varphi_k^2 \quad (1)$$

In doing so, it is easier to identify by visual inspection the direction of the flow of electron density and especially which orbital pairs correspond to donation and which to back-bonding.^[45] Pictorial representations of the deformation densities ΔQ_k calculated for complex **1** are depicted in Figure 4 along with the corresponding eigenvalues. For each of them, two representations are shown, orthogonal and parallel to the plane of the phen ligand. In particular, only the first four deformation densities (with the leading eigenvalues) are associated with bond channels (ΔQ_i , $i = 1–4$) and, as can be observed in Figure 4, ΔQ_2 and ΔQ_3 are related to the σ -donation from the phen ligand to the metal fragment and ΔQ_1 and ΔQ_4 represent metal-to-ligand π -back-donation (ΔQ_4 is better described as back-donation along with polarization). The same sequence of bond channels has been found for the other complexes of the series bearing substituted phenanthrolines. At this level of theory, the

only quantitative information is given by the eigenvalues ν_k associated with ΔQ_k , which are related to the magnitude of the charge transfer. As a consequence, eigenvalues related to ΔQ_2 and ΔQ_3 represent the flow of electron density associated with σ -donation from phen* to molybdenum (their sum gives Δq_σ with a positive value) and eigenvalues related to ΔQ_1 and ΔQ_4 represent the flow of electron density associated with Mo–phen* back-donation (their sum gives Δq_π with a negative value). The remaining deformation densities and the associated eigenvalues are related to the reorganization of electron density inside the fragments and are not directly coupled to bond channels. A complete list of the charge-transfer values (Δq_i) obtained by NOCV calculations is reported in Table S2 in the Supporting Information.

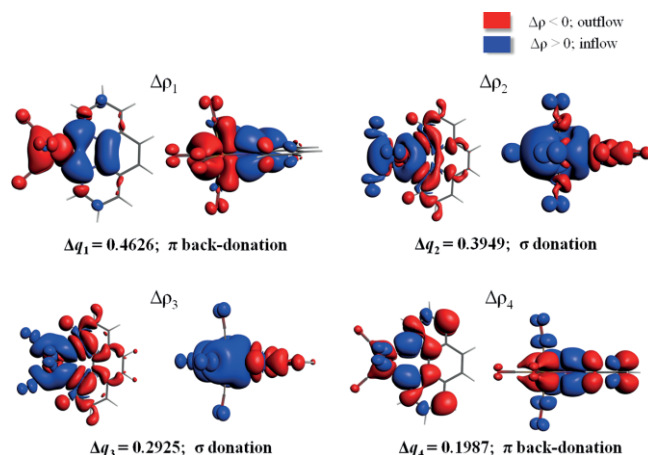


Figure 4. Contours of deformation density channels ΔQ_k describing the interactions between fragments in $[\text{Mo}(\text{CO})_4(\text{phen})]$ (**1**). Two different visualizations (orthogonal and parallel to the plane of the phen ligand) are depicted.

Table 2 presents the Δq_σ and Δq_π values for complexes **1–13**, together with the resulting Δq , which represents the amount of the overall flow and is obtained by the algebraic addition of Δq_σ and Δq_π : A negative sign for Δq signifies a net electron density transfer from fragment **F1** ($\{\text{Mo}(\text{CO})_4\}$, Figure 3) to fragment **F2** ($\{\text{phen}^*\}$), and thus denotes phen* ligands with a prevalence for π -acidic behavior. Reported in the last column of Table 2 are the values of Δq relative to 1,10-phenanthroline

Table 2. Charge-transfer magnitudes for complexes $[\text{Mo}(\text{CO})_4(\text{phen}^*)]$ **1–13**.

	phen*	Δq_σ ^[a]	Δq_π ^[b]	Δq ^[c]	$\Delta q^{\text{phen[d]}}$
1	phen	0.6874	−0.6613	0.0262	1.00
2	5-NO ₂ -phen	0.6813	−0.6901	−0.0088	−0.33
3	5-NH ₂ -phen	0.6915	−0.6571	0.0345	1.32
4	bathophen	0.6967	−0.6645	0.0322	1.23
5	4,7-Me ₂ -phen	0.6898	−0.6263	0.0635	2.43
6	tmphen	0.6955	−0.6187	0.0768	2.94
7	5,6-Me ₂ -phen	0.6915	−0.6516	0.0400	1.53
8	5-Me-phen	0.6868	−0.6522	0.0346	1.32
9	5-Cl-phen	0.6848	−0.6706	0.0142	0.54
10	5-Br-phen	0.6845	−0.6679	0.0166	0.63
11	4,7-Cl ₂ -phen	0.6826	−0.6804	0.0023	0.09
12	3,8-Br ₂ -phen	0.6787	−0.6892	−0.0105	−0.40
13	Br ₄ -phen	0.6786	−0.6994	−0.0209	−0.80

[a] Δq_σ represents σ -donation. [b] Δq_π represents π -back-donation. [c] $\Delta q = \Delta q_\sigma + \Delta q_\pi$. [d] $\Delta q^{\text{phen}} = \Delta q/0.0262$.

(Δq^{phen}), which has been arbitrarily assigned a value $\Delta q^{\text{phen}} = 1.00$. The resulting Δq^{phen} values are in good agreement with the qualitative explanation offered by the Dewar–Chatt–Duncanson model: phen* with electron-rich substituents show σ -donor ability ($\Delta q^{\text{phen}} > 1$) whereas phen* with electron-withdrawing groups are characterized by high π acidity ($\Delta q^{\text{phen}} < 1$). Interestingly, the plot of $\nu_{\text{CO}} (A_{1\text{ax}})$ versus Δq^{phen} (Figure 5) shows that all the considered compounds have a linear fit, which means that when the σ -donation and π -back-donation properties of these ligands are considered simultaneously (in this case, in the Δq^{phen} parameter), their contribution to the Mo–phen* bond can be quantitatively assessed.

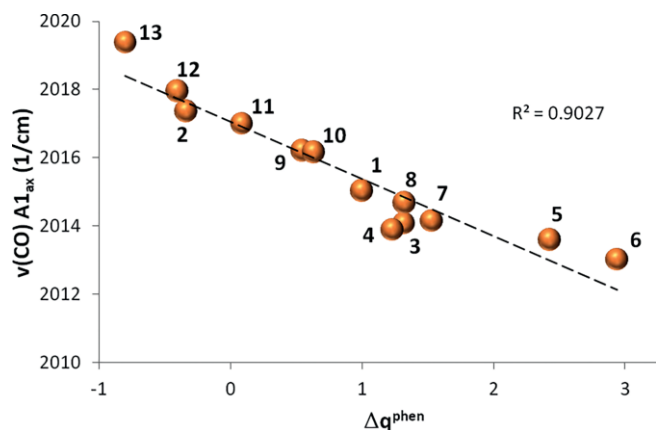


Figure 5. Plot of $\nu_{\text{CO}} (A_{1\text{ax}})$ vs. Δq^{phen} for compounds 1–13.

Energy Decomposition Analysis

Table 3 and Table 4 collect the results of the ETS analysis performed on complexes 1–13, and all the energies (ΔE_{1-4}) associated with each bond channel ($\Delta \rho_{1-4}$) can be found in Table S3 in the Supporting Information. ΔE_{prep} , which is the amount of energy required to promote the separated fragments **F1** and **F2** from their equilibrium geometry to the structure they will assume in the final complex, has not been calculated. Indeed, if one is not interested in the total bond energies ($\Delta E_{\text{total}} = -D_{\text{bond}}$), but only in describing the interfragment interactions

in terms of orbital (e.g., σ , π , δ) and electrostatic contributions, ΔE_{prep} can be ignored, focusing the attention merely on ΔE_{int} . For all the complexes, the largest contribution to ΔE_{int} comes from the attractive term ΔE_{elstat} with a ratio to ΔE_{orb} equal to about 1.80, which means that the Mo–phen* bond has more electrostatic (64–65 %) than covalent (35–36 %) character (with the largest electrostatic contribution belonging to phenanthrolines bearing electron-donating substituents in complexes **3**, **4**, and **6**).

Table 3. ETS-NOCV results describing the interactions between fragments **F1** and **F2** in the complexes $[\text{Mo}(\text{CO})_4(\text{phen}^*)]$.

	phen*	ΔE [kcal/mol]				% E_{orb}	% E_{elstat}
		$\Delta E_{\text{int}}^{[a]}$	ΔE_{orb}	ΔE_{Pauli}	ΔE_{elstat}		
1	phen	-59.70	-54.38	95.50	-100.82	35.00	65.00
2	5-NO ₂ -phen	-57.01	-54.05	95.04	-98.00	35.50	64.50
3	5-NH ₂ -phen	-60.50	-54.74	96.04	-101.80	35.00	65.00
4	bathophen	-61.11	-55.53	96.64	-102.22	35.20	64.80
5	4,7-Me ₂ -phen	-60.92	-54.03	94.03	-100.92	34.90	65.10
6	tmphen	-61.90	-55.13	96.67	-103.45	34.80	65.20
7	5,6-Me ₂ -phen	-60.74	-54.59	95.54	-101.69	34.90	65.10
8	5-Me-phen	-60.12	-53.84	93.85	-100.13	35.00	65.00
9	5-Cl-phen	-58.52	-54.05	94.75	-99.22	35.30	64.70
10	5-Br-phen	-58.54	-53.78	94.01	-98.77	35.30	64.70
11	4,7-Cl ₂ -phen	-57.97	-54.12	95.09	-98.93	35.40	64.60
12	3,8-Br ₂ -phen	-55.71	-53.19	92.25	-94.77	35.90	64.10
13	Br ₄ -phen	-54.28	-53.09	91.51	-92.71	36.40	63.60

[a] $\Delta E_{\text{int}} = \Delta E_{\text{orb}} + \Delta E_{\text{Pauli}} + \Delta E_{\text{elstat}}$.

Similarly, a general trend is also observed for the repulsive term ΔE_{Pauli} in which higher values are associated with compounds with electron-rich 1,10-phenanthrolines [i.e., 96.7 kcal/mol for $[\text{Mo}(\text{CO})_4(\text{tmphen})]$ (**6**)], whereas lower values are found for complexes with an electron-poor phen* [91.5 kcal/mol for $[\text{Mo}(\text{CO})_4(\text{Br}_4\text{-phen})]$ (**13**). The σ and π contributions to ΔE_{orb} are quite similar among the complexes, with a general prevalence for σ -donation ($\%E_{\sigma} \geq 57.5$) compared with π -back donation. The latter increases as expected in the presence of electron-poor phen*.

In the search for a possible quantitative description of the Mo–phen* bond, and bearing in mind the mutual synergistic action of the σ and π contributions, we plotted both the values of E_{σ} and E_{π} calculated for each compound against the corre-

Table 4. ETS-NOCV results describing the interaction between fragments **F1** and **F2** in the complexes $[\text{Mo}(\text{CO})_4(\text{phen}^*)]$.

	phen*	ΔE or E [kcal/mol]				$\Delta E_{\text{rest}}^{[a]}$	% E_{σ}	% E_{π}	% ΔE_{rest}
		ΔE_{orb}	E_{σ}	E_{π}					
1	phen	-54.38	-31.67	-12.04	-10.67	58.20	22.10	19.60	
2	5-NO ₂ -phen	-54.05	-31.13	-12.53	-10.39	57.60	23.20	19.20	
3	5-NH ₂ -phen	-54.74	-31.91	-11.98	-10.85	58.30	21.90	19.80	
4	bathophen	-55.53	-32.12	-12.36	-11.04	57.80	22.20	19.90	
5	4,7-Me ₂ -phen	-54.03	-31.70	-11.46	-10.86	58.70	21.20	20.10	
6	tmphen	-55.13	-32.09	-11.72	-11.32	58.20	21.30	20.50	
7	5,6-Me ₂ -phen	-54.59	-31.86	-11.89	-10.84	58.40	21.80	19.80	
8	5-Me-phen	-53.84	-31.43	-11.81	-10.61	58.40	21.90	19.70	
9	5-Cl-phen	-54.05	-31.41	-12.14	-10.50	58.10	22.50	19.40	
10	5-Br-phen	-53.78	-31.26	-12.06	-10.46	58.10	22.40	19.40	
11	4,7-Cl ₂ -phen	-54.12	-31.24	-12.36	-10.52	57.70	22.80	19.40	
12	3,8-Br ₂ -phen	-53.19	-30.73	-12.36	-10.11	57.80	23.20	19.00	
13	Br ₄ -phen	-53.09	-30.50	-12.53	-10.06	57.50	23.60	19.00	

[a] ΔE_{rest} is the sum of the intrafragment polarizations due to minor internal rearrangements (each <2 kcal/mol).

sponding experimental ν_{CO} , first focusing our attention on the $A_{1\text{ax}}$ vibrational mode. The result is a 3D graph (Figure 6) in which data are fitted with a plane, the least-squares regression of which leads to Equation (2) with a good correlation coefficient (adj. $R^2 = 0.9819$).

$$\nu_{\text{CO}} = 2081.51 + 2.882E_{\sigma} - 2.048E_{\pi} \quad (2)$$

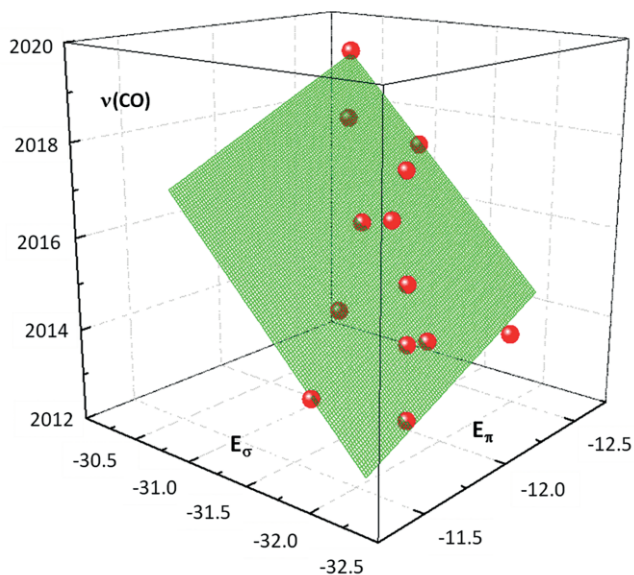


Figure 6. Plot of ν_{CO} ($A_{1\text{ax}}$ [cm^{-1}]) vs. E_{σ} and E_{π} (both expressed in kcal/mol) for compounds **1–13** (adj. $R^2 = 0.9819$).

Considering the negative (stabilizing) values of both E_{σ} and E_{π} , according to Equation (2) a higher basic character (i.e., higher E_{σ}) of the phen* ligand leads to a decrease in ν_{CO} , whereas an augment in π -back-bonding (higher E_{π}) causes an increase in the vibrational stretching value. Both these considerations are in accord with experimental observations. Moreover, from Equation (2), it is clear that the ν_{CO} stretching is influenced more by σ -donor ability than by π -back-bonding. A better visualization of this correlation can be obtained by including the E_{σ} and E_{π} energies for each compound in the corresponding terms in Equation (2): A new parameter is generated, $T(A_{1\text{ax}})$, which simultaneously includes the two (σ and π) bond interactions [e.g., $T(A_{1\text{ax}}) = 2.882(-31.67) - 2.048(-12.04) = -66.61$ kcal/mol for compound $[\text{Mo}(\text{CO})_4(\text{phen})]$ (**1**); see Table S4 in the Supporting Information]. As already done for Δq (see Figure 5), the $T(A_{1\text{ax}})$ parameter can be easily converted into the corresponding $T(A_{1\text{ax}})^{\text{phen}}$ by dividing it by the value of $T(A_{1\text{ax}})$ for 1,10-phenanthroline (-66.61 kcal/mol), once more taken as a reference for the series. The plot of $T(A_{1\text{ax}})^{\text{phen}}$ versus ν_{CO} ($A_{1\text{ax}}$) gives an excellent linear relationship (Figure 7). Worthy of note, similar outcomes were obtained when this procedure was applied to the remaining vibrational modes, thereby leading to the analogous parameters $T(B_1)^{\text{phen}}$, $T(A_{1\text{eq}})^{\text{phen}}$, and $T(B_2)^{\text{phen}}$ (see Table S4). The four parameters show comparable values for each complex, hence they can be averaged into a single, general parameter T^{phen} (Table 5).

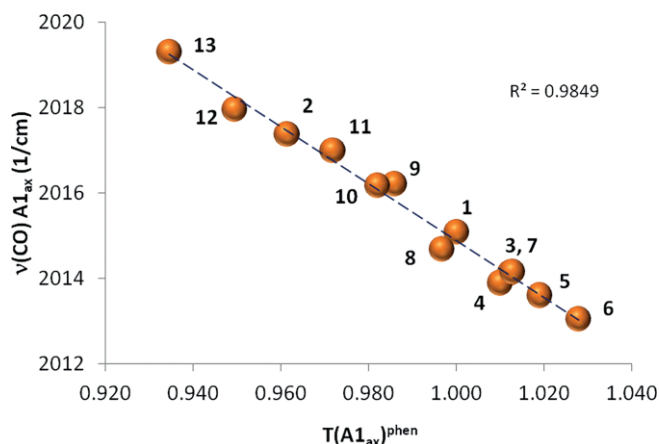


Figure 7. Linear relationship between $T(A_{1\text{ax}})^{\text{phen}}$ and ν_{CO} ($A_{1\text{ax}}$).

Table 5. Values of the comprehensive T^{phen} parameter for complexes **1–13**.

	phen*	T^{phen}
13	Br_4 -phen	0.923
12	3,8- Br_2 -phen	0.941
2	5- NO_2 -phen	0.952
11	4,7- Cl_2 -phen	0.966
10	5-Br-phen	0.980
9	5-Cl-phen	0.983
8	5-Me-phen	0.998
1	phen	1.000
4	bathophen	1.008
3	5- NH_2 -phen	1.014
7	5,6- Me_2 -phen	1.016
5	4,7- Me_2 -phen	1.027
6	tmphen	1.034

From the data reported in Table 5 it is evident that the T^{phen} parameter can be taken as a descriptor of the overall electronic properties of the phen* ligand: Values of $T^{\text{phen}} < 1$ are usually associated with phen* with π -acceptor substituents, whereas the presence of electron-rich substituents on phen* leads to enhancement of its E_{σ} contribution and eventually to $T^{\text{phen}} > 1$. Moreover, this parameter shows excellent accord with the experimental observations, as demonstrated by the good linear fits of T^{phen} with all four ν_{CO} modes measured for the corresponding complex in solution (Figure 8).

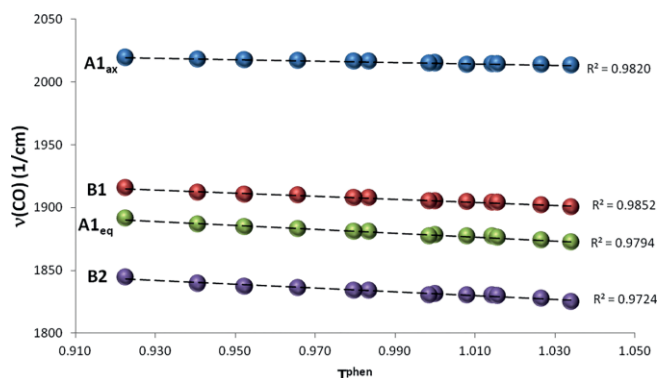


Figure 8. Linear relationship between T^{phen} and the four vibrational modes ν_{CO} in the series of complexes **1–13**.

The Case of 2,(9)-Substituted 1,10-Phenanthrolines

All the conclusions drawn on 7^{phen} in the previous paragraph are related to compounds containing 1,10-phenanthrolines with hydrogen atoms at the 2- and 9-positions. $[\text{Mo}(\text{CO})_4(\text{cupr})]$ (**14**), $[\text{Mo}(\text{CO})_4(2,9\text{-Cl}_2\text{-phen})]$ (**15**), and $[\text{Mo}(\text{CO})_4(2\text{-CN-phen})]$ (**16**) were initially discarded from this dissertation due to their odd behavior, outlined in Figures S1–S3 in the Supporting Information. Deviation from the common behavior observed for complexes **1–13** occurred in the geometry optimization of complex **14**. Indeed, intriguingly, the neocuproine-containing derivative $[\text{Mo}(\text{CO})_4(\text{cupr})]$ (**14**) was the only complex to give a different outcome, with the heterocyclic ligand being bent from the plane identified by Mo and the two equatorial CO ligands (see Figure S4). Similar results were also obtained by employing other functionals, such as B3LYP^[46] or M06.^[47] In contrast, geometry optimization of complexes **15** and **16** led to results comparable to those obtained for species **1–13**, without anomalous deformations in the molybdenum coordination sphere. To shed light on this aspect, to determine whether the structure of complex **14** really presents a “bent” phen or whether it is simply a computational artefact, we decided to perform a single-crystal X-ray structure analysis on complex **14**. The ORTEP plot of **14** is reported in Figure 9.

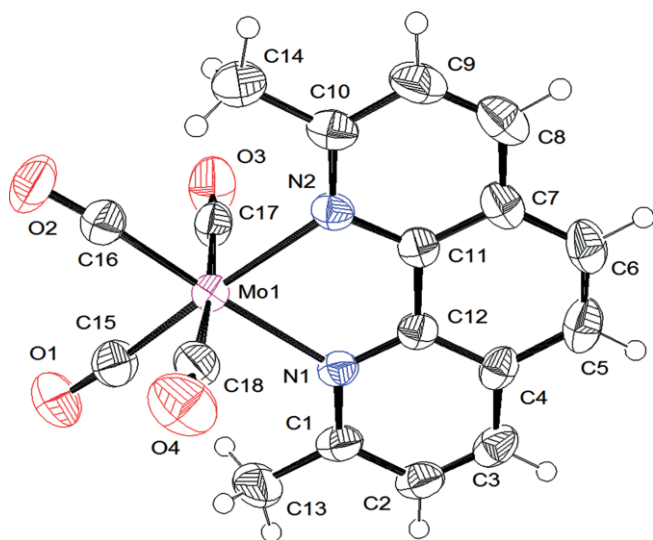


Figure 9. ORTEP representation of **14**. Ellipsoids are drawn at the 50 % probability level. Single crystals suitable for X-ray analysis were obtained by slow diffusion of hexane into a dichloromethane solution of **14**.

The molecular structure of **14** is quite similar to those reported for $[\text{Mo}(\text{CO})_4(\text{phen})]$ (**1**)^[44] and $[\text{Mo}(\text{CO})_4(\text{batho})]$ (**4**)^[48] showing the neocuproine to be coplanar with the plane of $\{\text{Mo}(\text{CO}_{\text{eq}})_2\}$. Regarding the distorted octahedral environment

around the molybdenum, some relevant differences (reasonably attributable to the greater steric hindrance of the methyl groups at the 2- and 9-positions) can be noticed in the structural parameters of **14** when compared with those of **1** and **4** (Figure 10). First, the Mo–N distances are longer in **14** than in **1** and **4** (ca. 2.30 vs. 2.24 Å). Next, the axial C–Mo–C angle (α in Figure 10) is very close to 180° in **14** [175.2(2)°], whereas in **1** and **4** these angles measure 167.6(2) and 170.4(8)°, respectively. Concurrently, the equatorial C–Mo–C angle (β) in **14** is the most acute among the series, being only 79.5(2)°, as compared with 93.2(1)° in **1** and 88.9(8)° in **4**. In addition, in the crystal packing, the heterocyclic ring is involved in π – π interactions (3.34 Å) with adjacent molecules, thus generating stacks of phenanthroline units along the *a* axis.

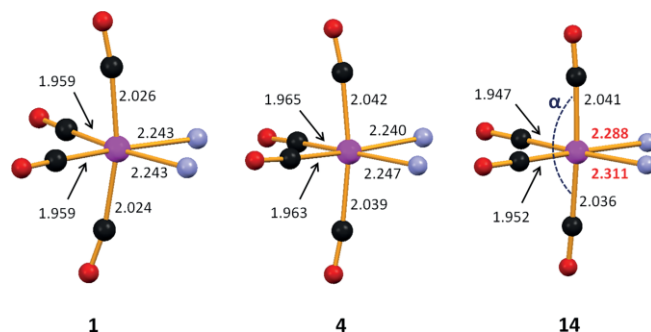


Figure 10. Main structural parameters in the octahedral cores of $[\text{Mo}(\text{CO})_4(\text{phen})]$ (**1**)^[44], $[\text{Mo}(\text{CO})_4(\text{batho})]$ (**4**)^[48] and $[\text{Mo}(\text{CO})_4(\text{cupr})]$ (**14**). Distances are in Å; the angles are as follows: $\alpha = 167.6(2)^\circ$ (**1**), $170.4(8)^\circ$ (**4**), and $175.2(2)^\circ$ (**14**).

A new geometry optimization for compound **14** was performed, starting from the crystal structure obtained at room temperature and accordingly by imposing a planar geometry on the $\{\text{Mo}(\text{CO}_{\text{eq}})_2(\text{neocuproine})\}$ moiety.^[49] The ETS-NOCV investigation was then performed on compounds **14–16** (see Tables S5 and S6 in the Supporting Information) starting from the newly optimized structures. The most relevant results are summarized in Table 6; for the complete set of ΔE_i and Δq_i data, see Tables S5 and S6 in the Supporting Information.

As found for compounds **1–13** (Table 3), the largest contribution to ΔE_{int} comes from the attractive term ΔE_{elstat} with a ratio to ΔE_{orb} ranging from 1.74 (**16**) to 1.89 (**14**), these being the highest values for the whole series. Thus, again, the Mo–phen* bond has more electrostatic (63.5–65.4 %) than covalent (34.6–36.5 %) character. One interesting feature emerges when the repulsive term, ΔE_{Pauli} is considered: $[\text{Mo}(\text{CO})_4(2,9\text{-Cl}_2\text{-phen})]$ (**15**) shows a value of 84.1 kcal/mol for ΔE_{Pauli} , the lowest for the whole $[\text{Mo}(\text{CO})_4(\text{phen}^*)]$ series and definitely quite far from the average (93.8 kcal/mol). For compounds **15** and **16**, the

Table 6. ETS-NOCV results describing the interaction between fragments **F1** and **F2** in complexes **14–16**.

	phen*	ΔE [kcal/mol]					% E_{orb}	% E_{elstat}	E [kcal/mol]	
		ΔE_{int}	ΔE_{orb}	ΔE_{Pauli}	ΔE_{elstat}	$\Delta E_{\text{rest}}^{\text{[a]}}$			E_{σ}	E_{π}
14	cupr	–57.13	–51.81	92.87	–98.18	–12.15	34.54	65.46	–28.59	–11.08
15	2,9-Cl ₂ -phen	–47.01	–47.56	84.06	–83.51	–10.86	36.29	63.71	–25.68	–11.03
16	2-CN-phen	–53.34	–53.08	92.20	–92.46	–10.60	36.47	63.53	–29.28	–13.26

[a] ΔE_{rest} is the sum of the intrafragment polarizations due to minor internal rearrangements (each <2 kcal/mol).

stabilizing term ΔE_{elstat} and the destabilizing ΔE_{Pauli} nearly cancel each other out, their sums being +0.55 (**15**) and -0.26 cal/mol (**16**), respectively. Consequently, in these cases ΔE_{int} shows a value very close to ΔE_{orb} . The σ and π contributions to ΔE_{orb} are quite similar among the complexes, with a general prevalence of σ -donation compared with π -back-donation. As expected, the E_{π} value is highest for the derivative containing the electron-withdrawing 2-CN-phen ligand.

These results validate the data obtained from the ETS-NOCV scheme applied to complexes **14–16**, which showed energies and quantities not dramatically dissimilar to those formerly calculated for **1–13**. This led us to suppose a possible fitting of the above-mentioned quantities to the previously obtained correlations (see Figures 5, 7, and 8). However, both the Δq versus $\nu_{\text{CO}}(A_{1\text{ax}})$ and the T^{phen} versus $\nu_{\text{CO}}(A_{1\text{ax}})$ plots (Figure 11) reveal a net deviation of these three complexes (**14–16**) from the general trend shown by the 2,9-unsubstituted species (**1–13**). Moreover, even when T^{phen} is plotted against the other vibrational modes (see Figure S5 in the Supporting Information), the values associated with complexes **14–16** always present odd behavior. This means that T^{phen} , which accounts for the electronic contributions due to σ -donation and π -back-donation in the Mo-phen* bond, cannot be used to give a quantitative description of the bond when 2,9-substituted phenanthrolines are consid-

ered. Reasonably, repulsion effects due to the sterically demanding 2(9)-substituents, well highlighted by the irregular behavior of the experimental stretching frequencies (see Figures S1–S3), would lead to distortions in solution that are hardly predictable in the optimized geometries.

Conclusions

This work aimed at giving a quantitative description of the bond between molybdenum and substituted 1,10-phenanthrolines (phen*) in the carbonyl complexes $[\text{Mo}(\text{CO})_4(\text{phen}^*)]$. By applying the ETS-NOCV method to the two interacting fragments in the compounds, $\{\text{Mo}(\text{CO})_4\}$ and $\{\text{phen}^*\}$, it has been possible to highlight both the σ -donation (i.e., E_{σ}) and π -back-donation (E_{π}) contribution of phen* to the metal–ligand Mo-phen* bond. Moreover, E_{σ} and E_{π} have been correlated with the experimental frequencies of the carbonyl ligands in solution: A good fit was attained when they were considered simultaneously, thus reflecting the synergistic action of σ and π contributions in the experimental observations. A new parameter (T^{phen}) was then introduced: T^{phen} has been demonstrated to be a reliable descriptor of the electronic (σ -donor and π -acceptor) properties of phen* ligands, with the exception of 2,9-substituted derivatives. In this latter case, the steric effects imposed by the 2,9-substitutions would probably lead to distortions in solution that are hardly predictable in the geometry optimization and consequently by the ETS-NOCV method. However, it is necessary to point out that differences in ancillary ligands and metal (i.e., in the metal-containing fragment) can cause significant differences in the acid/base (and steric) properties of the ligands.^[3b,45] Thus, before establishing a general trend, further studies are needed.

Experimental Section

General Procedures: All reactions were carried out under purified nitrogen using standard Schlenk techniques. Solvents were dried and distilled according to standard procedures prior to use. Elemental analyses were performed with a Perkin–Elmer CHN Analyzer 2400 Series II. IR spectra were recorded with a Shimadzu Prestige-21 spectrophotometer. 5-Nitro-1,10-phenanthroline (5-NO₂-phen)^[40] and 5-amino-1,10-phenanthroline (5-NH₂-phen)^[33] were prepared according to literature methods. All other chemicals were of reagent-grade quality, were purchased commercially (TCI Chemicals), and used as received.

General Procedure for the Synthesis of Compounds 1–16:^[41] A mixture of $[\text{Mo}(\text{CO})_6]$ (1 g, 3.79 mmol) and the 1,10-phenanthroline ligand (3.79 mmol) in toluene (25 mL) was stirred for 4 h at 80 °C. During this time the mixture first turned into a pink-red solution, then into a red-purple suspension. This suspension was filtered and the resulting orange-to-red precipitate was washed with pentane and then dried *in vacuo*. See Table S7 in the Supporting Information for further experimental details.

Computational Details: All calculations were carried out at the density functional (DFT) level of theory by using the ADF2014.2 program package.^[50] The hybrid functional PBE0^[42] was employed for geometry optimization. The PBE0 exchange correlation functional is based on the generalized gradient corrected exchange cor-

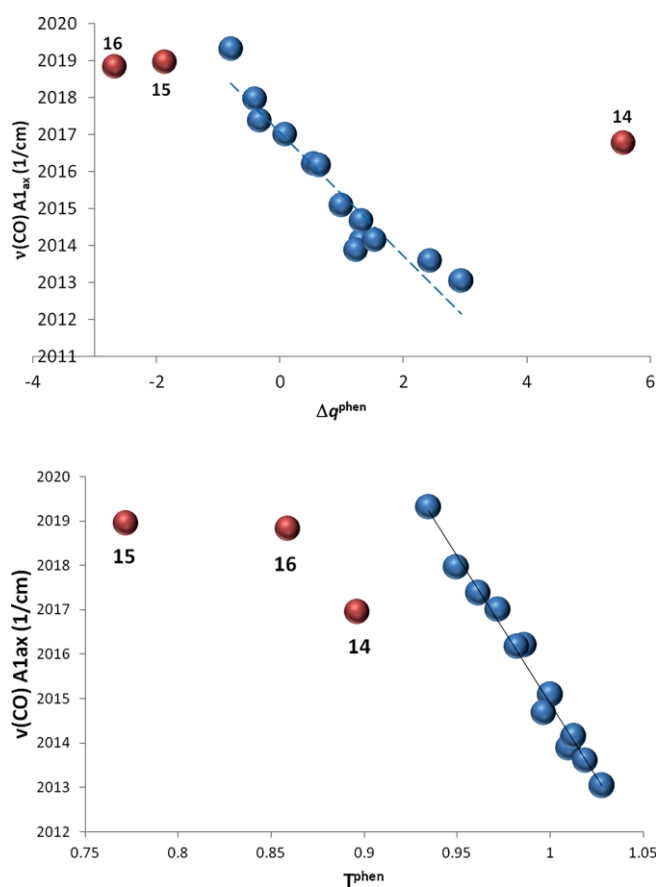


Figure 11. Deviation of the behavior of **14–16** (red dots) with respect to **1–13** (blue dots) in the Δq vs. $\nu_{\text{CO}}(A_{1\text{ax}})$ and T^{phen} vs. $\nu_{\text{CO}}(A_{1\text{ax}})$ plots.

relation functional of Perdew–Burke–Ernzerhof (PBE) with a fixed amount (25 %) of Hartree–Fock exchange energy. Restricted formalism was applied for all closed-shell systems (complexes and fragments). For geometry optimization and fragment analysis, C, H, N, O, and Cl atoms were described through TZ2P basis sets (triple- ζ STO plus two polarization functions), the QZ4P basis set (quadruple- ζ STO plus four polarization function) was used for Br and Mo atoms. The no-frozen-core approximation (all-electron) and no symmetry constraints were used in all calculations. The geometries of the complexes were optimized by simulating solvent effects (CH₂Cl₂) employing the conductor-like continuum solvent model (COSMO)^[51] as implemented in the ADF suite. Frequency calculations were performed for all optimized structures to establish the nature of the stationary points. Plots of calculated versus experimental $\nu(\text{CO})$ are presented in Figure S6 in the Supporting Information.

Single-Crystal X-ray Structure Analysis: A crystal of **14** was mounted on a Stoe Image Plate Diffraction system equipped with a ϕ circle goniometer using Mo- K_{α} graphite-monochromatic radiation ($\lambda = 0.71073 \text{ \AA}$) with a ϕ range of 0–180°. The structure was solved by direct methods using the program SHELXS-97, and the refinement and all further calculations were carried out by using SHELXL-97.^[52] The hydrogen atoms were included in the calculated positions and treated as riding atoms using the SHELXL default parameters. The non-hydrogen atoms were refined anisotropically by using weighted full-matrix least-squares on F^2 . Crystallographic details for **14** are summarized in Table S8 in the Supporting Information. Figure 9 was drawn with ORTEP.^[53]

CCDC 1469390 (for **14**) contains the supplementary crystallographic data for this paper. These data can be obtained free of charge from The Cambridge Crystallographic Data Centre.

Supporting Information (see footnote on the first page of this article): Experimental details for complexes **1–16**, data from the ETS-NOCV analyses, the equations and parameters $z0$, a , and b used in the least-squares regression analysis of the planes, plots of calculated versus experimental ν_{CO} for complexes **1–16**, atomic coordinates from geometry optimization, full list of authors for ref.^[50c]

Acknowledgments

This work was partially supported by the University of Insubria, Italy (grant number CSR-12).

Keywords: Molybdenum · Carbonyl ligands · Ligand effects · Density functional calculations · Nitrogen heterocycles

- [1] G. Frenking, N. Frölich, *Chem. Rev.* **2000**, *100*, 717–774.
 [2] P. L. Damon, C. J. Liss, R. A. Lewis, S. Morochnik, D. E. Szpunar, J. Tesler, T. W. Hayton, *Inorg. Chem.* **2015**, *54*, 10081–10095.
 [3] a) N. Fey, A. G. Orpen, J. N. Harvey, *Coord. Chem. Rev.* **2009**, *253*, 704–722; b) G. Frenking, K. Wichmann, N. Frölich, J. Grobe, W. Golla, D. Le Van, B. Krebs, M. Läge, *Organometallics* **2002**, *21*, 2921–2930.
 [4] T. Ziegler, A. Rauk, *Inorg. Chem.* **1979**, *18*, 1755–1759.
 [5] A. W. Ehlers, S. Dapprich, S. F. Vyboishchikov, G. Frenking, *Organometallics* **1996**, *15*, 105–117.
 [6] G. Pacchioni, P. S. Bagus, *Inorg. Chem.* **1992**, *31*, 4391–4398.
 [7] a) A. E. Reed, L. A. Curtiss, F. Weinhold, *Chem. Rev.* **1988**, *88*, 899–926; b) T. Leyssens, D. Peeters, A. G. Orpen, J. N. Harvey, *Organometallics* **2007**, *26*, 2637–2645.
 [8] C. H. Suresh, N. Koga, *Inorg. Chem.* **2002**, *41*, 1573–1578.

- [9] A. L. Fernandez, M. R. Wilson, A. Prock, W. P. Giering, *Organometallics* **2001**, *20*, 3429–3435.
 [10] a) M. P. Mitoraj, A. Michalak, *J. Mol. Model.* **2007**, *13*, 347–355; b) A. Michalak, M. P. Mitoraj, T. Ziegler, *J. Phys. Chem. A* **2008**, *112*, 1933–1939.
 [11] T. Ziegler, A. Rauk, *Theor. Chim. Acta* **1977**, *46*, 1–10.
 [12] a) M. P. Mitoraj, H. Zhu, A. Michalak, T. Ziegler, *Int. J. Quantum Chem. Theory Comput.* **2009**, *5*, 962–975; b) M. P. Mitoraj, R. Kurczab, R. Boczar, A. Michalak, *J. Mol. Model.* **2010**, *16*, 1789–1795; d) M. P. Mitoraj, *J. Phys. Chem. A* **2011**, *115*, 14708–14716; e) M. P. Mitoraj, M. Parafiniuk, M. Srebro, M. Handzlik, A. Buczek, A. Michalak, *J. Mol. Model.* **2011**, *17*, 2337–2352.
 [13] a) C. Werlé, D. M. Anstine, L. Karmazin, C. Bailly, L. Ricard, J.-P. Djukic, *Dalton Trans.* **2016**, *45*, 607–617; b) C. Werlé, L. Karmazin, C. Bailly, L. Ricard, J.-P. Djukic, *Organometallics* **2015**, *34*, 3055–3064; c) C. Werlé, C. Bailly, L. Karmazin-Brelot, X.-S. Le Goff, L. Ricard, J.-P. Djukic, *J. Am. Chem. Soc.* **2013**, *135*, 17839–17852.
 [14] a) M. Srebro, M. P. Mitoraj, *Organometallics* **2009**, *28*, 3650–3655; b) M. P. Mitoraj, A. Michalak, T. Ziegler, *Organometallics* **2009**, *28*, 3727–3733; c) I. Cukrowski, K. K. Govender, M. P. Mitoraj, M. Srebro, *J. Phys. Chem. A* **2011**, *115*, 12746–12758.
 [15] S.-W. Yeh, C.-W. Lin, B.-H. Liu, C.-C. Tsou, M.-L. Tsai, W.-F. Liaw, *Chem. Eur. J.* **2015**, *21*, 16035–16046.
 [16] H. Braunschweig, W. C. Ewing, T. Kramer, J. D. Mattock, A. Vargas, C. Werner, *Chem. Eur. J.* **2015**, *21*, 12347–12356.
 [17] V. H. L. Wong, A. J. P. White, T. S. A. Hor, K. K. Hii, *Chem. Commun.* **2015**, *51*, 17752–17755.
 [18] a) D. A. Safin, M. G. Babashkina, M. Bolte, M. P. Mitoraj, A. Klein, *Dalton Trans.* **2015**, *44*, 16824–16832; b) D. A. Safin, M. P. Mitoraj, K. Roybens, Y. Filinchuk, C. M. L. Vande Velde, *Dalton Trans.* **2015**, *44*, 14101–14109; c) D. A. Safin, M. G. Babashkina, K. Roybens, M. P. Mitoraj, P. Kubisiak, Y. Garcia, *Chem. Eur. J.* **2015**, *21*, 16679–16687.
 [19] J. C. Bernhammer, G. Frison, H. V. Huynh, *Chem. Eur. J.* **2013**, *19*, 12892–12905.
 [20] E. Broclawik, J. Załucka, P. Kozrya, M. Mitoraj, J. Datka, *Catal. Today* **2011**, *169*, 45–51.
 [21] a) M. P. Mitoraj, A. Michalak, *Struct. Chem.* **2012**, *23*, 1369–1375; b) M. P. Mitoraj, A. Michalak, *J. Mol. Model.* **2013**, *19*, 4681–4688.
 [22] K. Dyduch, M. P. Mitoraj, A. Michalak, *J. Mol. Model.* **2013**, *19*, 2747–2758.
 [23] M. Parafiniuk, M. P. Mitoraj, *Organometallics* **2013**, *32*, 4103–4113.
 [24] P. G. Hayes, Z. Xu, C. Beddie, J. M. Keith, M. B. Hall, T. D. Tilley, *J. Am. Chem. Soc.* **2013**, *135*, 11780–11783.
 [25] N. T. A. Nhung, N. Van Ly, D. Dien, P. J. Van Tat, *J. Sci. Technol.* **2014**, *52*, 483–487.
 [26] N. Holzmann, G. Frenking, *Croat. Chem. Acta* **2014**, *87*, 413–422.
 [27] I. Cukrowski, J. H. de Lange, M. Mitoraj, *J. Phys. Chem. A* **2014**, *118*, 623–637.
 [28] C. R. Landis, R. P. Hughes, F. Weinhold, *Organometallics* **2015**, *34*, 3442–3449.
 [29] S. Banerjee, *Theor. Chem. Acc.* **2016**, *135*, 20.
 [30] M. Bayat, M. Hatami, *Polyhedron* **2016**, *110*, 46–54.
 [31] H. Jacobsen, *Can. J. Chem.* **2016**, *94*, 149–154.
 [32] C. R. Luman, F. N. Castellano, “Phenanthroline Ligands”, in *Comprehensive Coordination Chemistry II*, 2nd ed., vol. 1 (Fundamentals: Ligands, Complexes, Synthesis, Purification, and Structure) (Eds.: T. J. Meyer, J. A. McCleverty), Elsevier Ltd. **2003**, pp. 25–39.
 [33] S. J. Lee, S. S. Lee, M. S. Lah, J.-M. Hong, J. H. Jung, *Chem. Commun.* **2006**, 4539–4541.
 [34] S. Akerboom, J. J. M. H. van den Elshout, I. Mutikainen, M. A. Siegler, W. T. Fu, E. Bouwman, *Eur. J. Inorg. Chem.* **2013**, 6137–6146.
 [35] K. J. Castor, K. L. Metera, U. M. Tefashe, C. J. Serpell, J. Mauzeroll, H. F. Sleiman, *Inorg. Chem.* **2015**, *54*, 6958–6967.
 [36] R. Johnson, H. Madhani, J. P. Bullock, *Inorg. Chim. Acta* **2007**, *360*, 3414–3423.
 [37] a) Q. Ye, Q. Wu, H. Zhao, Y.-M. Song, X. Xue, R.-G. Xiong, S.-M. Pang, G.-H. Lee, *J. Organomet. Chem.* **2005**, *690*, 286–290; b) L. Yang, J.-K. Feng, A.-M. Ren, *Synth. Met.* **2005**, *152*, 265–268; c) I. R. Farrell, F. Hartl, S. Zális, T. Mahabiersing, A. Vlček Jr., *J. Chem. Soc. Dalton Trans.* **2000**, 4323–4331.
 [38] a) D. M. Manuta, A. J. Lees, *Inorg. Chem.* **1983**, *22*, 3825–3828; b) D. M. Manuta, A. J. Lees, *Inorg. Chem.* **1986**, *25*, 1354–1359; c) S. Wieland, K. B.

- Reddy, R. van Eldik, *Organometallics* **1990**, *9*, 1802–1806; d) W.-F. Fu, R. van Eldik, *Organometallics* **1997**, *16*, 572–578; e) E. M. Lindsay, C. H. Langford, A. D. Kirk, *Inorg. Chem.* **1999**, *38*, 4771–4776.
- [39] M. P. T. Sjörgen, H. Frisell, B. Akermark, P.-O. Norrby, L. Eriksson, A. Vitagliano, *Organometallics* **1997**, *16*, 942–950.
- [40] S. Ji, H. Guo, X. Yuan, X. Li, H. Ding, P. Gao, C. Zhao, W. Wu, W. Wu, J. Zhao, *Org. Lett.* **2010**, *12*, 2876–2879.
- [41] M. H. I. Stiddard, *J. Chem. Soc.* **1962**, 4712–4715.
- [42] a) J. P. Perdew, K. Burke, M. Ernzerhof, *Phys. Rev. Lett.* **1996**, *77*, 3865–3868; erratum: J. P. Perdew, K. Burke, M. Ernzerhof, *Phys. Rev. Lett.* **1997**, *78*, 1396; b) J. P. Perdew, M. Ernzerhof, K. Burke, *J. Chem. Phys.* **1996**, *105*, 9982–9985; c) C. Adamo, V. Barone, *J. Chem. Phys.* **1999**, *110*, 6158–6170.
- [43] G. A. Ardizzoia, S. Brenna, S. Durini, B. Therrien, M. Veronelli, *Eur. J. Inorg. Chem.* **2014**, 4310–4319.
- [44] H. J. Bruins Slot, N. W. Murrall, A. J. Welch, *Acta Crystallogr., Sect. C* **1985**, *41*, 1309–1312.
- [45] M. P. Mitoraj, A. Michalak, *Inorg. Chem.* **2010**, *49*, 578–582.
- [46] a) A. D. Becke, *Phys. Rev. A* **1988**, *38*, 3098–3100; b) C. Lee, W. Yang, R. G. Parr, *Phys. Rev. B* **1988**, *37*, 785–789; c) A. D. Becke, *J. Chem. Phys.* **1993**, *98*, 5648–5652; d) P. J. Stephens, F. J. Devlin, C. F. Chabalowski, M. J. Frisch, *J. Phys. Chem.* **1994**, *98*, 11623–11627.
- [47] a) Y. Zhao, D. G. Truhlar, *J. Chem. Phys.* **2006**, *110*, 13126–13130; b) Y. Zhao, D. G. Truhlar, *Theor. Chem. Acc.* **2008**, *120*, 215–241.
- [48] X.-J. Xie, X.-L. Jin, K.-L. Tang, *Acta Crystallogr., Sect. C* **2001**, *57*, 696–697.
- [49] Constraints were necessary because, even starting from the experimental geometry, the optimization process has always led to a bent neocuproine.
- [50] a) G. te Velde, F. M. Bickelhaupt, E. J. Baerends, C. Fonseca Guerra, S. J. A. van Gisbergen, J. G. Snijders, T. Ziegler, *J. Comput. Chem.* **2001**, *22*, 931–967; b) C. Fonseca Guerra, J. G. Snijders, G. te Velde, E. J. Baerends, *Theor. Chem. Acc.* **1998**, *99*, 391–403; c) *ADF2014, SCM*, Theoretical Chemistry, Vrije Universiteit, Amsterdam, <http://www.scm.com>, see the Supporting Information for the complete reference.
- [51] a) A. Klamt, G. J. Schürmann, *J. Chem. Soc. Perkin Trans. 2* **1993**, *2*, 799–805; b) A. Klamt, V. Jonas, *J. Chem. Phys.* **1996**, *105*, 9972–9981; c) C.-C. Pye, T. Ziegler, *Theor. Chem. Acc.* **1999**, *101*, 396–408.
- [52] G. M. Sheldrick, *Acta Crystallogr., Sect. A* **2008**, *64*, 112–122.
- [53] L. Farrugia, *J. Appl. Crystallogr.* **1997**, *30*, 565.

Received: May 31, 2016

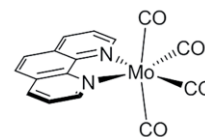
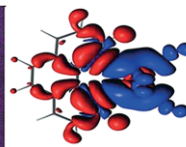
Published Online: ■

Substituted Phenanthrolines

G. A. Ardizzoia, M. Bea,
S. Brenna,* B. Therrien 1–10



A Quantitative Description of the σ -Donor and π -Acceptor Properties of Substituted Phenanthrolines



Like players of opponent teams in rugby, σ and π contributions are involved in a sort of “electronic scrum” that determines the nature of metal–ligand bonds. An ETS-NOCV study allowed us to quantify these contribu-

tions, associated with E_{σ} and E_{π} , in $[\text{Mo}(\text{CO})_4(\text{phen}^*)]$ compounds. A new electronic parameter (T^{phen}) comprising both E_{σ} and E_{π} has been introduced and correlated with experimental data.

DOI: 10.1002/ejic.201600647